A GNSS/5G Integrated Positioning Methodology in D2D Communication Networks

Lu Yin, *Member, IEEE*, Qiang Ni, *Senior Member, IEEE*, and Zhongliang Deng

***Abstract*— Global navigation satellite system (GNSS) is not suitable for the dense urban or indoor environments as the satellite signals are very weak. Meanwhile, positioning is an important application of the fifth-generation (5G) communication system. GNSS/5G integrated positioning system becomes a promising research topic with the development of 5G standard. This paper focuses on the integrated methodology of GNSS and device to device (D2D) measurements in 5G communication system. We analyze the characteristics of this type of integrated system and propose a high-efficiency D2D positioning measure protocol, named crossover multiple-way ranging, which consumes less communication resources. Then, to deal with the high-dimensional state space in the integrated system, a state dimension reduction method is proposed to overcome the particle degeneracy problem of particle filter which is used to fusion GNSS and 5G D2D measurements. Three integrated algorithms in different scenarios have been proposed: the first one is the integrated algorithm when the range measurements can be measured directly. The second one is the integrated algorithm with unknown time skew and offset of each mobile terminal. The third one is the integrated algorithm in GNSS-denied environment which is prevalent in urban and indoor applications. The simulation and experimental results show that our proposed integrated methodology outperforms the nonintegrated one.**

***Index Terms*— GNSS/5G integrated positioning, crossover multiple-way ranging, particle filter, dimension reduction, time uncertainty.**

I. Introduction

GLOBAL navigation satellite system (GNSS) can provide continuous position, velocity and time (PVT). In recent years, the performance of GNSS improves a lot thanks to the modernization of the U.S. global positioning system (GPS) and the Russian GLONASS, as well as the construction of the Chinese BeiDou navigation system (BDS) and the European Galileo [1], [2]. Nowadays, GNSS has been widely used in civil navigation, industrial equipment monitoring, intelligent transportations, etc [3], [4]. With the continuous increasing demand of location based services (LBS), high-accuracy and high-robustness positioning becomes more and more important. Because the satellite signals are very weak in the complicated environments, such as urban areas and inside buildings [5], [6], it is hard for GNSS to position accurately and continuously in these scenarios. Integrated positioning with other systems, such as the cellular positioning system [7], the WiFi positioning [8], the inertial navigation system (INS) [9], and so on, emerges as a promising solution to overcome the problem of GNSS.

With the emergence of the fifth generation (5G) communication systems, 5G positioning becomes a new research area. Cui *et al.* [10], [11] proposed positioning schemes by using 5G millimeter-wave (mmWave) signals. Peral-Rosado *et al.* [12] provided a study on 5G positioning for the assisted driving in vehicle-to-infrastructure networks and gave some simulation results. Dammann *et al.* [13] introduced a positioning algorithm based on signal level in 5G networks.

Specifically, as a new 5G technology, device to device (D2D) communication is more flexible, efficient and consumes lower power than other 5G techniques, which can be potentially used to obtain accurate relative range and angle measurements for positioning. With D2D measurements, any mobile terminal (MT) in the positioning network will be helped by all other MTs for a high-accurate positioning. The high-dense property of 5G networks also makes it easier to obtain sufficient D2D observations to achieve the *any-time* and *any-where* seamless positioning [14]. Cui *et al.* [11] and Dammann textitet al. [15] gave brief models of 5G D2D positioning and addressed some prospects on 5G positioning. Werner *et al.* [14] proposed a joint positioning estimate method when clock offset exists in 5G networks.

However, D2D itself only provides relative measurements, absolute position will not be obtained if all MTs' positions are unknown. GNSS/5G integrated positioning is a promising solution to overcome this problem as GNSS provides absolute positions. Meanwhile, it could be beneficial to improve the positioning accuracy and robustness by using the integrated system. To the best of our knowledge, there is little comprehensive research on the GNSS/5G D2D integrated positioning. In this paper, we aim to develop a new positioning technology to integrate the GNSS and 5G D2D measurements, which can provide more accurate and reliable positioning. Two challenging problems will be addressed in this paper:

Manuscript received July 3, 2017; revised December 31, 2017; accepted January 20, 2018. Date of publication February 8, 2018; date of current version March 29, 2018. This work was supported in part by the National High-tech Research and Development Program of China (863 Program) under Grant 2015AA124101 and in part by the European FP7 Programme CROWN Project under Grant PIRSES-GA-2013-610524. *(Corresponding author: Qiang Ni.)*

L. Yin is with the School of Electronic Engineering, Beijing University of Posts and Telecommunications, Beijing 100876, China, and also with the InfoLab21, Lancaster University, Lancaster LA1 4WA, U.K. (e-mail: inlu_mail@bupt.edu.cn).

Q. Ni is with the InfoLab21, School of Computing and Communications, Lancaster University, Lancaster LA1 4WA, U.K. (e-mail: q.ni@lancaster.ac.uk).

Z. Deng is with the Joint Center of GNSS, Chinese Ministry of Education, School of Electronic Engineering, Beijing University of Posts and Telecommunications, Beijing 100876, China (e-mail: dengzhl@bupt.edu.cn).

Color versions of one or more of the figures in this paper are available online at http://ieeexplore.ieee.org.

Digital Object Identifier 10.1109/JSAC.2018.2804223

The first challenging problem is the D2D positioning measure[1] procedure in 5G networks. As the 5G is still developing, there is not a standard developed for specifying the protocols of D2D positioning measure. On the other hand, time offset and time skew affect the positioning accuracy dramatically.[2] A specialized procedure for D2D positioning measure in 5G networks must be designed either for the measuring efficiency or for the time uncertainty elimination.

The second main problem is the GNSS/5G integrated algorithm. Particle filter (PF) is a non-parametric Bayesian filter which is widely used in non-linear and non-Gaussian data fusion [16]. PF is intended to integrate GNSS and 5G D2D measurements in this paper. In GNSS/5G D2D integrated positioning, there are more states and redundant information than single system. As a result, it will lead to particle degeneracy which reduces the performance of PF. On the other hand, range measurements can not be obtained as the clocks of different MTs are unknown which makes the integrated algorithm difficult to be developed.

To tackle the two problems, the main contributions of this paper are:

1) We explore the D2D measure procedures for positioning in 5G D2D communication networks. We develop a new solution for 5G D2D positioning by the proposed crossover multiple-way ranging (CO-MWR) protocol without consuming much communication resources;
2) We propose a novel GNSS/5G integrated positioning scheme based on PF. We derive the integrated algorithm based on a proposed integrated model. Then we propose a state dimension reduction method to overcome the low filtering efficiency with high-dimensional stated spaces. This methodology demands less computation without losing much information;
3) We develop a series of algorithms based on the proposed integrated model which include the certain time parameters, uncertain time parameters and the GNSS-denied scenarios.

The paper is organized as follows: Section I gives an introduction of GNSS and 5G integrated positioning. Section II analyzes the characteristics of the GNSS/5G D2D integrated positioning and describes the proposed CO-MWR protocol. Section III gives the GNSS/5G integrated positioning model and derives the integrated algorithm. Section IV proposes an integrated method with the time uncertainties. Section V evaluates the performance of the proposed methodology via simulation and experiment results. Finally, the conclusions are given in VI.

Notations: $x^{(i)}$ means parameter x of MT i; $y^{(ij)}$ means parameter y between MT i and MT j measured by MT i (please notice the difference between $y^{(ij)}$ and $y^{(ji)}$). I_M, $\mathbf{0}_{M\times N}$ and $\mathbf{1}_{M\times N}$ represent the $M \times M$ identity matrix, the $M \times N$ matrix of zeros and ones, respectively. The operator $*$ and $\otimes$ represent the convolution and Kronecker product, respectively. $\|\cdot\|$ represents the Euclidean distance. diag $[A, B]$ means a matrix which diagonal elements are A and B, and the rest of this matrix are zeros. $\overset{\approx}{\propto}$ represents approximate proportional.

[1]D2D positioning measure represents the D2D range and angle measure for positioning in this paper.

[2]For example, 10ns time offset will lead to 3m range measurement error.

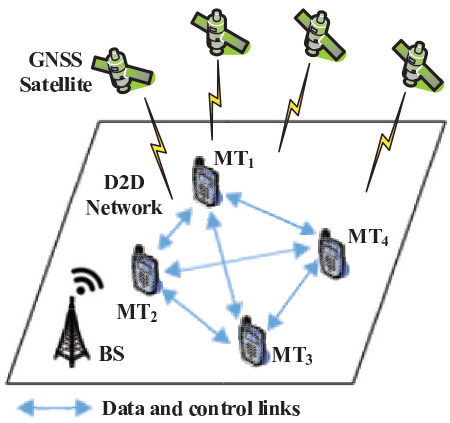

Fig. 1. GNSS/5G D2D integrated positioning network.

II. The D2D Positioning Measure Procedure in 5G Network

Consider a typical GNSS/5G D2D integrated positioning network as shown in Fig. 1. The MTs can communicate with each other known as D2D communication besides communicating with base stations (BSs) [11], [15]. When a MT wants to set up a D2D communication with another MT, D2D discovery, link evaluation, resources allocation and other relevant procedures will be firstly implemented via control link. Then, the data link of D2D communication will be set up and the data will be transmitted. D2D measure for positioning mainly has the following differences from the normal D2D communication:

1) Multi connection versus single connection. More measurements usually mean higher accuracy in integrated positioning. Therefore, a MT "wants" to do D2D positioning measure with as many as MTs "simultaneously". While a D2D communication only supports one pair of connection;
2) Frequent versus continuous. The user needs the positioning results frequently, such as 1Hz in GNSS. Despite the measure process, such as the signal tracking, the D2D positioning measure can be executed frequently. While the D2D communication usually needs to hold the connection continuously for a period;
3) Small amount versus huge amount of data. There is much fewer data needed for positioning application than communication purpose. Only few parameters need to be exchanged between two MTs, such as the range/angle measurements, GNSS outputs, statistical data and so on. While huge amount of data can be transmitted over D2D communications, such as voice, audio, video data and so on.

According to these differences, it is unnecessary to do the D2D positioning measure by the data link which means the

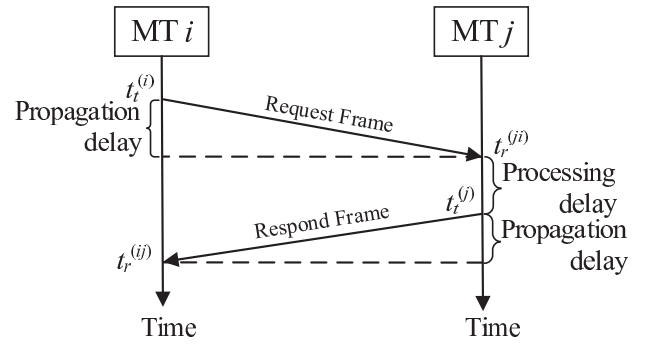

(a) Process of two-way ranging

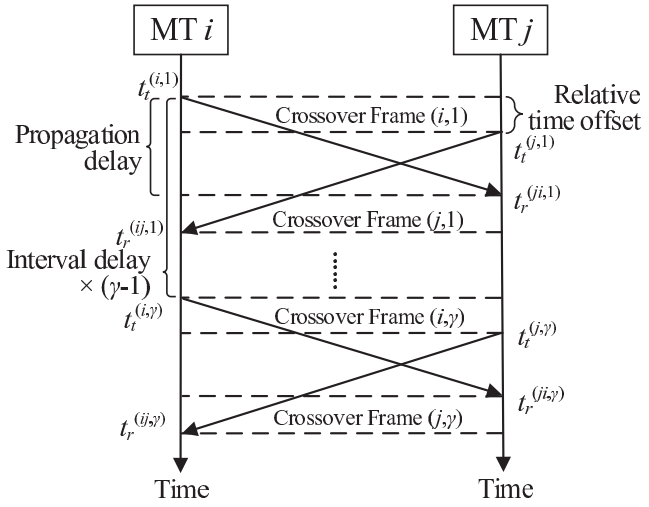

(b) Process of crossover multiple-way ranging

Fig. 2. Process of the traditional TWR and improved CO-MWR protocols.

D2D communication does not need to be truly set up for positioning application. Firstly, setting up a D2D communication consumes lots of resources and time. After connecting, little data is transmitted. Then, the connection will be released to do the next pair of D2D positioning measure. Hence, in our proposed protocol, the control link is used to do the D2D positioning measure.

In this paper, we mainly focus on the range measure procedure as the angle measurements can be obtained by MIMO technology directly via receiving the control signals [17], [18]. Distance between two MTs is obtained by analyzing propagation delays of the D2D signals. Two-way ranging (TWR) method in IEEE 802.15.4a is suitable for D2D range measure [11], [19]. The brief process of TWR is illustrated in Fig. 2a. Assuming the propagation delays of the request and respond frames are the same, the distance between two MTs is:

$$d^{(ij)} = \frac{1}{2}\left[\left(\frac{t_r^{(ij)} - t_t^{(i)}}{s^{(i)}}\right) - \left(\frac{t_t^{(j)} - t_r^{(ji)}}{s^{(j)}}\right)\right] c \qquad (1)$$

where t_t is the transmitting time, t_r is the receiving time, s is the clock skew, c is the light speed. Notice that the distance in (1) is measured by MT i, if MT j needs the measurement, another round of TWR frames is needed. So there are $2N(N-1)$ frames to be transferred, where N, $N \geq 2$, is the total amount of MTs in the positioning network. To improve the communication efficiency and save the terminals' power, we developed a crossover multiple-way ranging (CO-MWR) protocol as shown in Fig. 2b.

If there are positioning requests in the network,[3] MTs in this integrated network will transmit a Crossover Frame (CF) in the same time which is synchronized by GNSS 1PPS (pulse per second) timing signals. Notice that there are relative time offsets between any two MTs introduced by the GNSS timing errors, the absolute transmitting time is asynchronous as shown in Fig. 2b. After receiving the CFs, MTs do not respond immediately. They will wait for a known interval delay Δ_T and then transmit another CF. Then, the distance between two MTs in CO-MWR is calculated as:

$$d^{(ij)} + n_d^{(ij,\gamma)} = \left[\left(\frac{t_r^{(ij,\gamma)} - o^{(i)}}{s^{(i)}}\right) - \left[\frac{(\gamma - 1)\,\Delta_T - o^{(j)}}{s^{(j)}}\right]\right] c \qquad (2)$$

$$d^{(ij)} + n_d^{(ji,\gamma)} = \left[\left(\frac{t_r^{(ji,\gamma)} - o^{(j)}}{s^{(j)}}\right) - \left[\frac{(\gamma - 1)\,\Delta_T - o^{(i)}}{s^{(i)}}\right]\right] c \qquad (3)$$

where n_d is the range measurement error, o is the time offset which is not included in TWR as it is eliminated by the difference of transmitting and receiving time. $\gamma = 1, 2, \ldots, \Gamma$ is the measure time-label within a position update period.[4] Because the receiving time is local time, it must be switched to the absolute time firstly. Meanwhile, the transmitting time is not included in (2) and (3) which is replaced by a default time interval. As the signal is transmitted based on the local clock, it must be switched to the absolute time too.

Unlike TWR, all MTs will obtain the range and other information via any CF pairs in CO-MWR without additional measure rounds. It is because that the time-stamps do not need to be exchanged between the MTs as only the receiving time is included in (2) and (3). Suppose the amount of CF pairs is set to Γ in CO-MWR, then ΓN CFs are needed. Fig. 3 illustrates the comparison between TWR and CO-MWR on the measurement accuracy and the resource consumption, both of which increase with the increasing of Γ. Notice that $2N(N-1)$ frames are needed in TWR as aforementioned, so the CO-MWR costs less resources when $\Gamma < 2(N-1)$ (Region 1 and 3 in Fig. 3). Besides, higher D2D measurement accuracy will be obtained by CO-MWR when $\Gamma > 2$ (Region 1 and 2 in Fig. 3). So CO-MWR has the same or better performance on both measurement accuracy and resource consumption when $2 \leq \Gamma \leq 2(N-1)$ (Region 1 and two dashed lines in Fig. 3). On the other hand, let the measurement

[3]The requests can be initiated by the MTs which want to do D2D positioning measure, or a master MT in the network which gathers the positioning information.

[4]A position update period is typically equal to the GNSS output period. Normally, we can obtain more accurate measurements with more measures assuming time offset and skew are known and ignoring the MT's movements in the update period. However, more measures will cost more resources and power. A moderate number of measures are implemented by balancing the measurement accuracy and the cost of resources.

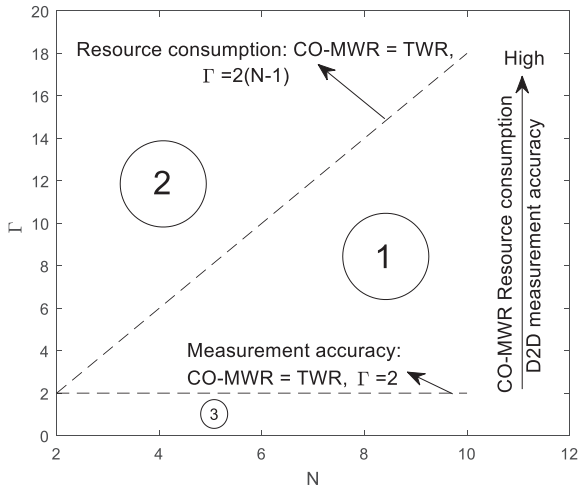

①: **HIGHER** measurement accuracy and **LESS** resource consumption by CO-MWR

②: **HIGHER** measurement accuracy but more resource consumption by CO-MWR

③: Lower measurement accuracy but **LESS** resource consumption by CO-MWR

Fig. 3. Comparison between CO-MWR and TWR on the measurement accuracy and the resource consumption.

accuracy of TWR be equivalent to the one of CO-MWR, then $\Gamma N(N-1)$, Γ is an even number, frames are needed in TWR. So CO-MWR always has better performance than TWR as ΓN is always smaller than $\Gamma N(N-1)$ as long as $N > 2$ under this condition.

III. Proposed GNSS/5G D2D Integrated Positioning Scheme

In this section, a GNSS/5G D2D integrated positioning scheme is proposed. The GNSS and 5G D2D measurements are integrated by a PF for a more accurate and robust position than single system. We assume all MTs in the integrated network are involved into the positioning application. For a particular MT, the input information includes 1) its own GNSS measurements at the integration time; 2) other MTs' integrated positioning results at the previous integration time (information at this time will be received via the next frames); and 3) the D2D range and angle measurements.

A. Particle Filter

Particle filter [20] is a kind of non-parametric form of Bayes filters. The posterior will be drawn by a finite number of particles after the importance sampling. When the amount of the particles is infinite, the posterior drawn by these particles will be the true one. With the finite particles, the posterior at time slot k is approximated as:

$$p\left(x_k \mid y_{1:k}\right) \approx \sum_{m=1}^{N_p} w_k\left(m\right) \delta\left(x_k - px_k(m)\right) \tag{4}$$

where x is the state, y is the measurements. px is the particles and $w\left(m\right)$ is the normalized weight of each particle. $\delta\left(\cdot\right)$ is the Dirac delta function. N_P is the amount of particles. According to the sequential Bayes theory, the posterior at time slot k is determined by the measurements likelihood, the prediction distribution and the posterior of the previous time slot $k-1$ as shown in (5). Thus, the posterior can be calculated recursively if we know the initial prior distribution of the state $p\left(x_0\right)$.

$$p\left(x_k \mid y_{1:k}\right) \propto p\left(y_k \mid x_k\right) p\left(x_k \mid x_{k-1}\right) \cdot p\left(x_{k-1} \mid y_{1:k-1}\right) \tag{5}$$

Because the posterior is usually different to be sampled, a known distribution q is selected to converge to the posterior as shown in (6).

$$q\left(x_k \mid y_{1:k}\right) = q\left(x_k \mid x_{k-1}, y_k\right) q\left(x_{k-1} \mid y_{1:k-1}\right) \tag{6}$$

Then, the weights are:

$$w_k\left(m\right) \propto \frac{p\left(x_k \mid y_{1:k}\right)}{q\left(x_k \mid y_{1:k}\right)} \propto \frac{p\left(y_k \mid x_k\right) p\left(x_k \mid x_{k-1}\right)}{q\left(x_k \mid x_{k-1}, y_k\right)} w_{k-1}\left(m\right) \tag{7}$$

where $q\left(x_k \mid x_{k-1}, y_k\right)$ is known as the importance distribution. For most particles, the weights are nearly zeros because they are in the low probability area of the posterior. After several time slots, no one would be close to the true state. To avoid this phenomenon, we can increase the amount of the particles. Or, more practically, we can resample the particles to keep the higher weight particles and discard the lower ones. After resampling, every particle will have the same weight. In practice, the importance distribution is often chosen as $q\left(x_k \mid x_{k-1}, y_k\right) = p\left(x_k \mid x_{k-1}\right)$. Then, (7) becomes:

$$w_k\left(m\right) \propto p\left(y_k \mid x_k\right) \tag{8}$$

Thus, the filtering result is:

$$\hat{x}_k = \frac{1}{N_p} \sum_{m=1}^{N_p} px_k\left(m\right) \tag{9}$$

B. Integrated GNSS/5G D2D Positioning by Particle Filter

Denote $\mathcal{M}$ as the set of MTs in the integrated positioning network, $\mathcal{N}^{(i\in\mathcal{M})}$ as the set of visible MTs of MT i, $\mathcal{N}^{(i^2)}$ as $\mathcal{N}^{(i)} \cup i$. Thus, $\mathcal{N}^{(i)} \subset \mathcal{N}^{(i^2)} \subseteq \mathcal{M}$. Denote $\Im = \{\gamma \mid \gamma = 1, 2, \ldots, \Gamma\}$ as the set of CFs within a position update period, and k as the GNSS output time. If $j \in \mathcal{N}^{(i)}$, $i\mathcal{N}^{(i)}$ represents all ijs, that is $i\mathcal{N}^{(i)} \in \left\{i1, i2, \ldots, ij, \ldots, j \in \mathcal{N}^{(i)}\right\}$. Please notice that $j \neq i$.

The integrated positioning is formulated as the following: find the posterior distribution of the MT's state $X^{(i)}$ with the whole information collected before k by MT i as shown in (10).

$$\text{bel}\left(X_k^{(i)}\right) = p\left(X_k^{(i)} \mid \mathcal{I}_{1:k}^{(i\mathcal{N}^{(i^2)})}\right), \quad \forall i \in \mathcal{M} \tag{10}$$

where $\mathcal{I}$ is the collected information at corresponding time. $\mathcal{I}_k^{(ii)}$ includes the GNSS measurement of MT i ($y_{G,k}^{(i)}$), the D2D measurements between MT i and all MT js in $\mathcal{N}^{(i)}$ ($y_{D,k}^{(i\mathcal{N}^{(i)},\Im)}$) measured by all CFs and their statistical data. $\mathcal{I}_k^{(ij)}$ includes the estimate state of MT j at time $k-1$ ($\hat{X}_{k-1}^{(j)}$) and its statistical data. Then, the $X_k^{(i)}$ which makes a maximum of bel$\left(X_k^{(i)}\right)$ is the integrated position. bel$\left(X_k^{(i)}\right)$ can be expressed in (11), as shown at the bottom of the next page.

If it is given an input bel$\left(X_{k-1}^{(\mathcal{N}^{(i^2)})}\right)$, the direct method for finding bel$\left(X_k^{(i)}\right)$ in PF is to draw the joint posterior distribution (the first two items of (11)). Then, we sum the joint posterior distribution to a marginal one. The integrated method is shown in Algorithm 1.

Algorithm 1 GNSS/5G D2D Integrated Positioning by Using Particle Filter

Input: The initial distribution at time slot 0.
Output: The estimate of $\hat{X}_k^{(i)}$.
1: For each particle $i = 1, 2, \ldots, N_P$, sample the initial state $PX_{X0}^{(\mathcal{N}^{(i^2)})}(m)$ from the initial distribution $p\left(X_0^{(\mathcal{N}^{(i^2)})}\right)$;
2: Calculate the weights and normalize them.
3: **for** time slot $k = 1, 2, 3, \ldots$ **do**
4: Sample the particles of time slot k by the importance distribution: $PX_k^{(\mathcal{N}^{(i^2)})}(m) \sim q\left(X_k^{(\mathcal{N}^{(i^2)})} \mid X_{k-1}^{(\mathcal{N}^{(i^2)})}\right)$;
5: Calculate the weights: $w_{p,k}^{(\mathcal{N}^{(i^2)})}(m) \propto p\left(y_{G,k}^{(i)}, \hat{X}_{k-1}^{(\mathcal{N}^{(i)})}, y_{D,k}^{(i\mathcal{N}^{(i)},\Im)} \mid X_k^{(\mathcal{N}^{(i^2)})}\right)$
6: Normalize the weights: $w_{p,k}^{(\mathcal{N}^{(i^2)})}(m) = w_{p,k}^{(\mathcal{N}^{(i^2)})}(m) / \sum_{m=1}^{N_p} w_{p,k}^{(\mathcal{N}^{(i^2)})}(m)$
7: Resampling and update the particle set $PX_k^{(\mathcal{N}^{(i^2)})}(m)$, then the weights become: $w_{p,k}^{(\mathcal{N}^{(i^2)})}(m) = \frac{1}{N_p}$
8: Project the particles to the $\hat{X}_k^{(i)}$ dimension, the new marginal particles are $PX_k^{(i)}(m)$. Then, the integrated state is $\hat{X}_k^{(i)} = \frac{1}{N_p}\sum_{m=1}^{N_p} PX_k^{(i)}(m)$
9: **end for**

Notice that $X_k^{(\mathcal{N}^{(i^2)})}$ is related to the size of $\mathcal{N}^{(i^2)}$. Thus, the state space is a high-dimensional variable which means it needs huge amount of particles to draw the joint distribution [21]. Because the MT usually has limited computational resources, it is impossible to use huge amount of particles to estimate the user's state. Thus, we propose a dimension reduction method to integrate these information in lower dimensional space.

C. State Dimension Reduction

Multiple particle filtering (MPF) uses several separate PFs by splitting the high-dimensional state space into several low-dimensional sub-spaces [22]. However, MPF can not substantially reduce the amount of particles as each individual PF needs plenty of particles as well. Moreover, individual PFs will lose the constraint information carried by D2D measurements. For a particular MT, what it concerns is its own state, our work focuses on the positioning MT's state by reducing the other MTs' state dimensions without losing much information.

Denote the intermediate state (IS) by:

$$Z_k^{(ij)} \sim p\left(z_k^{(ij)} = x_{x,k}^{(j)} - C_r^f\left(l_k^{(ij)}\right) \mid X_{x,k}^{(j)} = x_{x,k}^{(j)}, L_k^{(ij)} = l_k^{(ij)}\right) \tag{12}$$

where X_x is the position component in X, $L_k^{(ij)} = \left[d_k^{(ij)}, \eta_k^{(ij)}, \theta_k^{(ij)}\right]^T$ represents the distance, azimuth angle and elevation angle, respectively. $C_r^f(\cdot)$ is the transformation operator of the relative frame to the fixed frame as shown in (13):

$$C_r^f\left(l_k^{(ij)}\right) = \begin{bmatrix} d_k^{(ij)}\cos\left(\theta_k^{(ij)}\right)\cos\left(\eta_k^{(ij)}\right) \\ d_k^{(ij)}\cos\left(\theta_k^{(ij)}\right)\sin\left(\eta_k^{(ij)}\right) \\ d_k^{(ij)}\sin\left(\theta_k^{(ij)}\right) \end{bmatrix} \tag{13}$$

Denotes y_{Gx} as the position component in y_G, and $y_{Z,k}^{(ij,\gamma)} = y_{Gx,k}^{(j)} - C_r^f\left(y_{D,k}^{(ij,\gamma)}\right)$. Because the measurements $y_{Gx,k}^{(j)}$ and $y_{D,k}^{(ij,\gamma)}$ are independent, so the posterior of IS is:

$$p\left(y_{Z,k}^{(ij,\gamma)} \mid Z_k^{(ij)}\right) \propto p\left(y_{Gx,k}^{(j)} \mid X_{x,k}^{(j)}\right) * p\left(-C_r^f\left(y_{D,k}^{(ij,\gamma)}\right) \mid L_k^{(ij)}\right) \tag{14}$$

Then, by using the following constraint:

$$C_r^f\left(L_k^{(ij)}\right) = X_{x,k}^{(j)} - X_{x,k}^{(i)} \tag{15}$$

the posterior of IS becomes:

$$p\left(y_{Z,k}^{(ij,\gamma)} \mid Z_k^{(ij)}\right) \propto p\left(y_{Gx,k}^{(j)} \mid X_{x,k}^{(j)}\right) * p\left(-C_r^f\left(y_{D,k}^{(ij,\gamma)}\right) \mid X_{x,k}^{(j)} - X_{x,k}^{(i)}\right) \tag{16}$$

Notice that we do not have $y_{Gx,k}^{(j)}$ as the D2D CFs are received early than the GNSS output. So we use the received integrated position $\hat{X}_{k-1}^{(j)}$ instead of $y_{Gx,k}^{(j)}$ as $y_{Gx,k}^{(j)} = f_k^{(j)}\left(\hat{X}_{x,k-1}^{(j)}, u_{k-1}^{(j)}\right)$, where $f_k^{(j)}\left(\hat{X}_{x,k-1}^{(j)}, u_{k-1}^{(j)}\right) = A_{G,k}^{(j)}\hat{X}_{x,k-1}^{(j)} + \Phi_k^{(j)}u_{k-1}^{(j)}$ is the state transition function with the control input $u_{k-1}^{(j)}$, such as the velocities and accelerations. Then, the bel$\left(X_k^{(i)}\right)$ in (11) can be calculated in (17), as shown at the bottom of the next page assuming the process noise is

$$\begin{aligned} \text{bel}\left(X_k^{(i)}\right) &= \int p\left(X_k^{(\mathcal{N}^{(i^2)})} \mid \mathcal{I}_{1:k}^{(i\mathcal{N}^{(i^2)})}\right) \partial X_k^{(\mathcal{N}^{(i)})} \\ &\propto \int \underbrace{p\left(y_{G,k}^{(i)}, \hat{X}_{k-1}^{(\mathcal{N}^{(i)})}, y_{D,k}^{(i\mathcal{N}^{(i)},\Im)} \mid X_k^{(\mathcal{N}^{(i^2)})}\right)}_{\text{Likelihood of information}} \underbrace{p\left(X_k^{(\mathcal{N}^{(i^2)})} \mid X_{k-1}^{(\mathcal{N}^{(i^2)})}\right)}_{\text{Prediction}} \underbrace{\text{bel}\left(X_{k-1}^{(\mathcal{N}^{(i^2)})}\right)}_{\text{posterior of last time slot}} \partial X_k^{(\mathcal{N}^{(i)})} \end{aligned} \tag{11}$$

much less than the measurement noise. Notice that event $Z_k^{(ij)}$ is equivalent to event $X_{x,k}^{(i)}$ under the constraint (15) as:

$$p\left(Z_k^{(ij)} = z_k^{(ij)} \mid X_{x,k}^{(i)} = x_{x,k}^{(i)}\right) = \begin{cases} 1, & z_k^{(ij)} = x_{x,k}^{(i)} \\ 0, & z_k^{(ij)} \neq x_{x,k}^{(i)} \end{cases} \quad (18)$$

Thus, the bel $\left(X_k^{(i)}\right)$ is:

$$\begin{aligned} \text{bel}\left(X_{x,k}^{(i)}\right) &\overset{\approx}{\propto} p\left(y_{Gx,k}^{(i)}, y_{Z,k}^{(i\mathcal{N}^{(i)},\Im)} \mid X_{x,k}^{(i)}\right) \\ &\quad \cdot p\left(X_{x,k}^{(i)} \mid X_{x,k-1}^{(i)}, u_{k-1}^{(i)}\right) \text{bel}\left(X_{x,k-1}^{(i)}\right) \end{aligned} \quad (19)$$

It is shown in (19) that the joint distribution of $p\left(y_{G,k}^{(i)}, \hat{X}_{k-1}^{(\mathcal{N}^{(i)})}, y_{D,k}^{(i\mathcal{N}^{(i)},\Im)} \mid X_k^{(\mathcal{N}^{(i^2)})}\right)$ in Algorithm 1 (Step 5) do not need to be drawn. It means that the dimensions have been reduced from $6N$ to 3 in the 3-dimensional coordinate, where N is the size of $\mathcal{N}^{(i^2)}$. The cost of the reduction is we ignore the process noises of all MT j, and the impact of $X_{x,k-1}^{(i)}$ on other MT's belief. Although these operation will weaken the integrated performance, it has a crucial superiority in reducing the implementation complexity of PF.

If the time skew and offset are known, the integrated position can be estimated directly with the proposed algorithm as shown in Algorithm 2.

Algorithm 2 Integrated Algorithm for GNSS/5G D2D Integrated Positioning - Certain Time Parameters Scenario

Input: The initial distribution at time slot 0.
Output: The estimate of $\hat{X}_{x,k}^{(i)}$.
1: For each particle $i = 1, 2, \ldots, N_P$, sample the initial state $PX_0^{(i)}(m)$ from the initial distribution $p\left(X_{x,0}^{(i)}\right)$
2: Calculate the weights and normalize them.
3: **for** time slot $k = 1, 2, 3, \ldots$ **do**
4: Sample the particles of time slot k by the importance distribution: $PX_k^{(i)}(m) \sim p\left(X_{x,k}^{(i)} \mid X_{x,k-1}^{(i)}, u_{k-1}^{(\mathcal{N}^{(i)})}\right)$
5: Generate the ISs: $y_{Z,k}^{(i\mathcal{N}^{(i)},\Im)} = A_{G,k}^{(\mathcal{N}^{(i)},\Im)} \hat{X}_{x,k-1}^{(\mathcal{N}^{(i)})} + \Phi_k^{(\mathcal{N}^{(i)},\Im)} u_{k-1}^{(\mathcal{N}^{(i)})} - C_r^f\left(y_{D,k}^{(i\mathcal{N}^{(i)},\Im)}\right)$, where $A_{G,k}^{(\mathcal{N}^{(i)},\Im)}$ and $\Phi_k^{(\mathcal{N}^{(i)},\Im)}$ are given in (29) and (30), respectively.
6: Calculate the weights: $w_{p,k}^{(i)}(m) \propto p\left(y_{Gx,k}^{(i)}, y_{Z,k}^{(i\mathcal{N}^{(i)},\Im)} \mid X_{x,k}^{(i)}\right)$
7: Normalize the weights: $w_{p,k}^{(i)}(m) = w_{p,k}^{(i)}(m) / \sum_{m=1}^{N_p} w_{p,k}^{(i)}(m)$
8: Resampling and update the particle set $PX_k^{(i)}(m)$, then the weights become: $w_{p,k}^{(i)}(m) = \frac{1}{N_p}$
9: The integrated state is $\hat{X}_{x,k}^{(i)} = \frac{1}{N_p} \sum_{m=1}^{N_p} PX_k^{(i)}(m)$
10: **end for**

IV. Elimination of the Time Uncertainties

In practice, the time skew and offset are sometimes unknown. Then we do not have the range measurements. Before integration, the time uncertainties must be eliminated firstly. In the TWR, various protocols have been designed for time synchronization, such as the timing-sync protocol for sensor networks [23] and wireless arbitration protocol of the medium access control (MAC) layer [24]. A joint time synchronization and localization method was proposed in [25] which considers the synchronization problem and positioning problem in a unique framework. Because the time-based positioning and time synchronization are tightly coupled, the joint synchronization methods outperforms in many circumstances [26], [27]. In our proposed GNSS/5G D2D integrated positioning system, with the help of GNSS outputs and angle measurements, we can achieve a clear relationship between the positions and time uncertainties.

A. Elimination Model

Take (2) into $y_{Z,k}^{(ij,\gamma)}$ as shown in (20), as shown at the top of the next page, where y_η and y_θ are the measurement values of η and θ, respectively, T is the GNSS update interval. Denote $\vartheta^{(i)} = 1/s^{(i)}$ and $\vartheta^{(ij)} = [1/s^{(j)}, o^{(i)}/s^{(i)} + o^{(j)}/s^{(j)}]^T, i \neq j$. Take (20) into (13) and write it into matrix form, after rearranging the items, then we have:

$$\begin{aligned} y_{Z,k}^{(ij,\Im)} &= A_{G,k}^{(j,\Im)} \hat{X}_{x,k-1}^{(j)} + \Phi_k^{(j,\Im)} u_{k-1}^{(j)} \\ &\quad - \Omega_k^{(ij,\Im)} \left(A_{D,k}^{(ij,\Im)} \vartheta^{(i)} + B_{D,k}^{(ij,\Im)} \vartheta^{(ij)}\right) \end{aligned} \quad (21)$$

where

$$A_{G,k}^{(j,\Im)} = \mathbf{1}_{\Gamma\times 1} \otimes A_{G,k}^{(j)} \quad (22)$$

$$\Phi_k^{(j,\Im)} = \mathbf{1}_{\Gamma\times 1} \otimes \Phi_k^{(j)} \quad (23)$$

$$A_{D,k}^{(ij,\Im)} = c\left[t_{r,k}^{(ij,1)}, \ldots, t_{r,k}^{(ij,\Gamma)}\right]^T \otimes \mathbf{1}_{3\times 1} \quad (24)$$

$$\begin{aligned} \text{bel}\left(X_{x,k}^{(i)}\right) &\propto \int p\left(y_{Gx,k}^{(i)}, f_k^{(\mathcal{N}^{(i)})}\left(\hat{X}_{x,k-1}^{(\mathcal{N}^{(i)})}, u_{k-1}^{(\mathcal{N}^{(i)})}\right), y_{D,k}^{(i\mathcal{N}^{(i)},\Im)} \mid X_{x,k}^{(\mathcal{N}^{(i^2)})}, u_{k-1}^{(\mathcal{N}^{(i)})}\right) \\ &\quad \cdot p\left(X_{x,k}^{(\mathcal{N}^{(i^2)})} \mid X_{x,k-1}^{(\mathcal{N}^{(i^2)})}, u_{k-1}^{(\mathcal{N}^{(i^2)})}\right) \partial X_{x,k}^{(\mathcal{N}^{(i)})} \text{bel}\left(X_{x,k-1}^{(\mathcal{N}^{(i^2)})}\right) \\ &\propto \int p\left(C_r^f\left(y_{D,k}^{(i\mathcal{N}^{(i)},\Im)}\right) \mid X_{x,k}^{(\mathcal{N}^{(i)})} - X_{x,k}^{(i)}\right) p\left(f_k^{(\mathcal{N}^{(i)})}\left(\hat{X}_{x,k-1}^{(\mathcal{N}^{(i)})}, u_{k-1}^{(\mathcal{N}^{(i)})}\right) \mid X_{x,k}^{(\mathcal{N}^{(i)})}, u_{k-1}^{(\mathcal{N}^{(i)})}\right) \\ &\quad \cdot p\left(X_{x,k}^{(\mathcal{N}^{(i)})} \mid X_{x,k-1}^{(\mathcal{N}^{(i)})}, u_{k-1}^{(\mathcal{N}^{(i)})}\right) \partial X_{x,k}^{(\mathcal{N}^{(i)})} p\left(y_{Gx,k}^{(i)} \mid X_{x,k}^{(i)}\right) p\left(X_{x,k}^{(i)} \mid X_{x,k-1}^{(i)}, u_{k-1}^{(i)}\right) \text{bel}\left(X_{x,k-1}^{(\mathcal{N}^{(i^2)})}\right) \\ &\overset{\approx}{\propto} p\left(y_{Z,k}^{(i\mathcal{N}^{(i)},\Im)} \mid Z_k^{(i\mathcal{N}^{(i)})}\right) p\left(y_{Gx,k}^{(i)} \mid X_{x,k}^{(i)}\right) p\left(X_{x,k}^{(i)} \mid X_{x,k-1}^{(i)}, u_{k-1}^{(i)}\right) \text{bel}\left(X_{x,k-1}^{(\mathcal{N}^{(i^2)})}\right) \end{aligned} \quad (17)$$

$$y_{Z,k}^{(ij,\gamma)} = f_k^{(j)}\left(\hat{X}_{x,k-1}^{(j)}, u_{k-1}^{(j)}\right) - C_r^f\left(\left[\left(\left(\frac{t_{r,k}^{(ij,\gamma)} - o^{(i)}}{s^{(i)}}\right) - \left(\frac{(k-1)\,T + (\gamma - 1)\,\Delta_T - o^{(j)}}{s^{(j)}}\right)\right)c,\, y_{\eta,k}^{(ij,\gamma)},\, y_{\theta,k}^{(ij,\gamma)}\right]\right) \quad (20)$$

$$B_{D,k}^{(ij,\Im)} = c\begin{bmatrix} (1-k)\,T + (1-1)\,\Delta_T & 1 \\ \vdots & \vdots \\ (1-k)\,T + (1-\Gamma)\,\Delta_T & 1 \end{bmatrix} \otimes \mathbf{1}_{3\times 1} \quad (25)$$

$$\Omega_k^{(ij,\Im)} = \mathrm{diag}\left[\Omega_k^{(ij,1)}, \ldots, \Omega_k^{(ij,\Gamma)}\right] \quad (26)$$

where $\Omega_k^{(ij,\gamma)}$ is shown in (27), as shown at the bottom of the next page. Stacking (21) for all $N-1$ MTs in $\mathcal{N}^{(i)}$, noting $j = \jmath(n), n \in 1, 2, \ldots, N-1$, then we have (28), as shown at the bottom of the next page, where

$$A_{G,k}^{(\mathcal{N}^{(i)},\Im)} = \mathrm{diag}\left[A_{G,k}^{(\jmath(1),\Im)}, \ldots, A_{G,k}^{(\jmath(N-1),\Im)}\right] \quad (29)$$

$$\Phi_k^{(\mathcal{N}^{(i)},\Im)} = \mathrm{diag}\left[\Phi_{G,k}^{(\jmath(1),\Im)}, \ldots, \Phi_{G,k}^{(\jmath(N-1),\Im)}\right] \quad (30)$$

$$D_{D,k}^{(i\mathcal{N}^{(i)},\Im)} = \Omega_k^{(i\mathcal{N}^{(i)},\Im)}\left[A_{D,k}^{(i\mathcal{N}^{(i)},\Im)}, B_{D,k}^{(i\mathcal{N}^{(i)},\Im)}\right] \quad (31)$$

$$\Omega_k^{(i\mathcal{N}^{(i)},\Im)} = \mathrm{diag}\left[\Omega_k^{(i\jmath(1),\Im)}, \ldots, \Omega_k^{(i\jmath(N-1),\Im)}\right] \quad (32)$$

$$\vartheta^{(i\mathcal{N}^{(i)})} = \left[\vartheta^{(i)}, \vartheta^{(i\jmath(1))T}, \ldots, \vartheta^{(i\jmath(N-1))T}\right]^T \quad (33)$$

where

$$A_{D,k}^{(i\mathcal{N}^{(i)},\Im)} = \left[A_{D,k}^{(i\jmath(1),\Im)T}, \ldots, A_{D,k}^{(i\jmath(N-1),\Im)T}\right]^T \quad (34)$$

$$B_{D,k}^{(i\mathcal{N}^{(i)},\Im)} = \mathrm{diag}\left[B_{D,k}^{(i\jmath(1),\Im)}, \ldots, B_{D,k}^{(i\jmath(N-1),\Im)}\right] \quad (35)$$

Unlike using either a least squares based estimator or a factor graph to find the position and time uncertainties [25], [26], we use an orthogonal projection operator $\Psi_k^{(i)}$ to the orthogonal space of $D_{D,k}^{(i\mathcal{N}^{(i)},\Im)}$, which satisfies: $\Psi_k^{(i)} D_{D,k}^{(i\mathcal{N}^{(i)},\Im)} = 0$, to eliminate the time uncertainties. Notice that $D_{D,k}^{(i\mathcal{N}^{(i)},\Im)T} D_{D,k}^{(i\mathcal{N}^{(i)},\Im)}$ is not a full rank matrix which does not have an inverse, so we use the pseudo inverse to calculate. Then, the orthogonal projection matrix of $D_{D,k}^{(i\mathcal{N}^{(i)},\Im)}$ is $D_{D,k}^{(i\mathcal{N}^{(i)},\Im)}\left(D_{D,k}^{(i\mathcal{N}^{(i)},\Im)T} D_{D,k}^{(i\mathcal{N}^{(i)},\Im)}\right)^+ D_{D,k}^{(i\mathcal{N}^{(i)},\Im)T}$, and we have:

$$\Psi_k^{(i)} = I - D_{D,k}^{(i\mathcal{N}^{(i)},\Im)}\left(D_{D,k}^{(i\mathcal{N}^{(i)},\Im)T} D_{D,k}^{(i\mathcal{N}^{(i)},\Im)}\right)^+ D_{D,k}^{(i\mathcal{N}^{(i)},\Im)T} \quad (36)$$

where $(\cdot)^+$ represents the Moore-Penrose generalized pseudo inverse. As a result, (28) becomes:

$$\Psi_k^{(i)} y_{Z,k}^{(i\mathcal{N}^{(i)},\Im)} = \Psi_k^{(i)}\left(A_{G,k}^{(\mathcal{N}^{(i)},\Im)}\hat{X}_{k-1}^{(\mathcal{N}^{(i)})} + \Phi_k^{(\mathcal{N}^{(i)},\Im)} u_{k-1}^{(\mathcal{N}^{(i)})}\right) \quad (37)$$

B. Elimination Errors Compensation

The elimination of time uncertainties changes the distribution of the measurement errors. Actually, the orthogonal projection operator $\Psi_k^{(i)}$ makes the range measurements vector to collapse to the origin and compresses the measurement and state spaces as shown in (38).

$$p\left(y_{Gx,k}^{(i)}, \Psi_k^{(i)} y_{Z,k}^{(i\mathcal{N}^{(i)},\Im)} \mid X_{x,k}^{(i)}\right) = p\left(C_k^{(i)} X_{x,k}^{(i)} + n_{y,k}^{(i)}\right) \quad (38)$$

where $C_k^{(i)}$ is denoted as the alternative measurement matrix as shown in (39). $n_{y,k}^{(i)}$ is the equivalent measurement noise which satisfies (40). As (40) shows, $n_{y,k}^{(i)}$ is determined by two kinds of noises: one is caused by the GNSS measurement errors of each MTs ($n_{y_{Gx},k}^{(i)}$ and $n_{y_{Gx},k}^{(\mathcal{N}^{(i)},\Im)}$). The other is the residual error of the orthogonal projection ($n_{D_D,k}^{(i\mathcal{N}^{(i)},\Im)}$) caused by the D2D measurements noises.

$$C_k^{(i)} = \begin{bmatrix} I_{3\times 3} \\ \Psi_k^{(i)}\left(\mathbf{1}_{\Gamma(N-1)\times 1} \otimes I_{3\times 3}\right) \end{bmatrix} \quad (39)$$

$$n_{y,k}^{(i)} = \begin{bmatrix} n_{y_{Gx},k}^{(i)} \\ \Psi_k^{(i)}\left(n_{y_{Gx},k}^{(\mathcal{N}^{(i)},\Im)} + n_{D_D,k}^{(i\mathcal{N}^{(i)},\Im)}\right) \end{bmatrix} \quad (40)$$

1) The GNSS Measurement Errors of Each MTs: $n_{y_{Gx},k}^{(i)}$ is the GNSS measurement noise of MT i. $n_{y_{Gx},k}^{(\mathcal{N}^{(i)},\Im)}$ includes the estimate errors of MT $j \in \mathcal{N}^{(i)}$ at $k-1$ time slot ($n_{\hat{X},k-1}^{(\mathcal{N}^{(i)})}$), the errors of control input $n_{u,k-1}^{(\mathcal{N}^{(i)})}$ and the process noise ($V_k^{(\mathcal{N}^{(i)})}$) as shown in (41).

$$n_{y_{Gx},k}^{(\mathcal{N}^{(i)},\Im)} = A_{G,k}^{(\mathcal{N}^{(i)},\Im)} n_{\hat{X},k-1}^{(\mathcal{N}^{(i)})} + \Phi_k^{(\mathcal{N}^{(i)},\Im)} n_{u,k-1}^{(\mathcal{N}^{(i)})} + V_k^{(\mathcal{N}^{(i)})} \otimes \mathbf{1}_{\Gamma\times 1} \quad (41)$$

2) The Residual Error of the Orthogonal Projection: Denote $\Delta\Omega_k^{(i\mathcal{N}^{(i)},\Im)}$ as the error of $\Omega_k^{(i\mathcal{N}^{(i)},\Im)}$, then we have (42), as shown at the bottom of the next page, where $C_{D,k}^{(i\mathcal{N}^{(i)},\Im)} = \left[A_{D,k}^{(i\mathcal{N}^{(i)},\Im)}, B_{D,k}^{(i\mathcal{N}^{(i)},\Im)}\right]$, $\mathring{\Omega}$ and $\mathring{D}_D$ are the values without measurement errors of Ω and D_D, respectively. $\Psi_k^{(i)}\mathring{D}_{D,k}^{(i\mathcal{N}^{(i)},\Im)}$ would be expected to 0, so $n_{\Psi,k}^{(i)}$ is the error caused by the angle measurements. Because $C_{D,k}^{(i\mathcal{N}^{(i)},\Im)}\vartheta^{(i\mathcal{N}^{(i)})}$ are the distances between MT i and other MTs, we must estimate the distances firstly. Least square (LS) is employed to estimate the rough position of MT i as shown in (43).

$$\tilde{X}_{x,k}^{(i)} = \left(C_k^{(i)T} C_k^{(i)}\right)^{-1} C_k^{(i)T} y_{G,Z,k}^{(i\mathcal{N}^{(i)},\Im)} \quad (43)$$

where $y_{G,Z,k}^{(i\mathcal{N}^{(i)},\Im)} = \left[y_{Gx,k}^{(i)T}, \Psi_k^{(i)} y_{Z,k}^{(i\mathcal{N}^{(i)},\Im)T}\right]^T$. Then,

$$n_{\Psi,k}^{(i)} \approx \Psi_k^{(i)} \Delta\Omega_k^{(i\mathcal{N}^{(i)},\Im)} \tilde{d}_k^{(i\mathcal{N}^{(i)},\Im)} \quad (44)$$

where

$$\Delta\Omega_k^{(i\mathcal{N}^{(i)},\Im)} = \mathrm{diag}\left[\Delta\Omega_k^{(i\jmath(1),\Im)}, \ldots, \Delta\Omega_k^{(i\jmath(N-1),\Im)}\right] \quad (45)$$

$$\tilde{d}_k^{(i\mathcal{N}^{(i)},\Im)} = \left[\tilde{d}_k^{(i\jmath(1),\Im)T}, \ldots, \tilde{d}_k^{(i\jmath(N-1),\Im)T}\right]^T \quad (46)$$

where

$$\Delta\Omega_k^{(ij,\Im)} = \mathrm{diag}\left[\Delta\Omega_k^{(ij,1)}, \ldots, \Delta\Omega_k^{(ij,\Gamma)}\right] \quad (47)$$

$$\tilde{d}_k^{(ij,\Im)} = \left\|\tilde{X}_{x,k}^{(i)} - \left(A_{G,k}^{(j)}\hat{X}_{x,k-1}^{(j)} + \Phi_k^{(j)} u_{k-1}^{(j)}\right)\right\| \mathbf{1}_{3\Gamma\times 1} \quad (48)$$

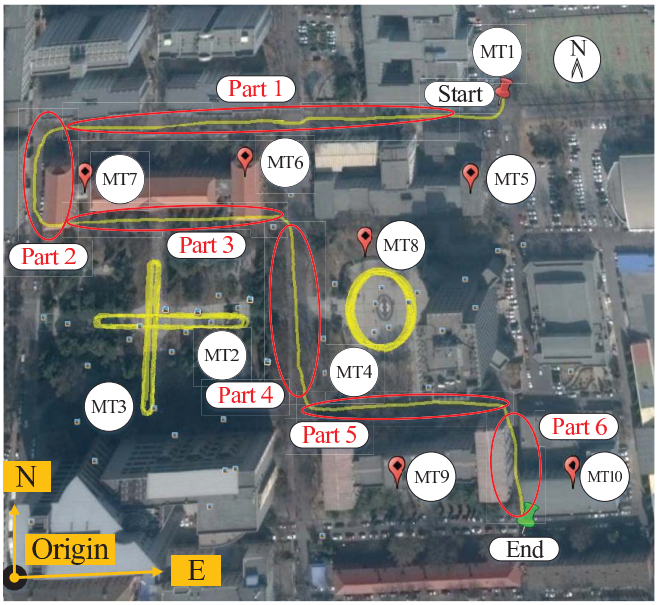

Fig. 4. Experiment Trajectories and location of each MT in BUPT campus.

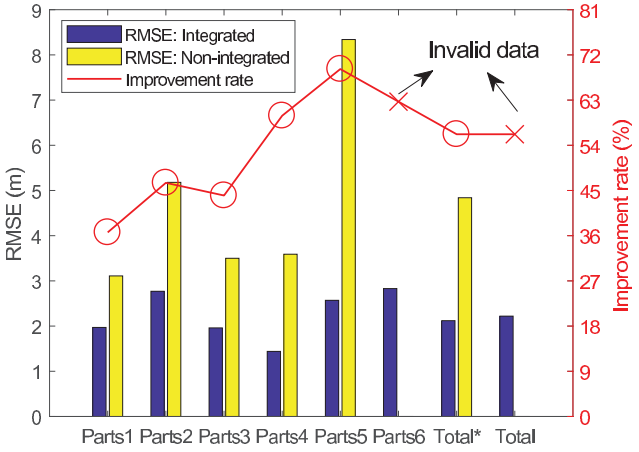

Fig. 5. Performance comparison between integrated and non-integrated in different trajectory parts (*Results excluding Part 6).

where $\Delta\Omega_k^{(ij,\gamma)}$ is the first order Taylor expansion of $\Omega_k^{(ij,\gamma)}$ at $y_{\theta,k}^{(ij,\gamma)}$ and $y_{\eta,k}^{(ij,\gamma)}$ as shown in (49), as shown at the bottom of this page. (44) includes two approximations: one is the approximation of $\Delta\Omega_k^{(ij,\gamma)}$ as we ignored the higher-order items in Taylor expansion. The other is the approximation of $\tilde{d}_k^{(ij,\Im)}$ which includes the rough estimation errors of the MTs' states. These approximations introduce higher-order errors of the estimated state which can be ignored in the PF. Comparing (40) and (44), then we have:

$$n_{D_D,k}^{(i\mathcal{N}^{(i)},\Im)} = \Delta\Omega_k^{(i\mathcal{N}^{(i)},\Im)} \tilde{d}_k^{(i\mathcal{N}^{(i)},\Im)} \tag{50}$$

At last, we can use the distributions of the original measurements to estimate the distribution of the equivalent measurement by (40) and (50). The integration algorithm with unknown time parameters is summarized in Algorithm 3.

V. Simulation and Experiment

The proposed algorithm is evaluated by several post-processing experiments with a set of real GNSS data and a set of generated 5G D2D data. The GNSS data were collected by our experimental platform equipped with a low-cost GNSS receiver - Ublox-M8N and a centimeter level accuracy RTK receiver - Huace X90 for reference. The 5G D2D data were generated by a software simulator[5] because there are not real 5G signals.

We walked around the campus of Beijing University of Posts and Telecommunications (BUPT) with the experimental platform (MT1) for data collection. The trajectory is shown in Fig. 4. The trajectory is divided into 6 parts: Parts 1, 3 and 4 have a well GNSS condition; Part 2 is between two buildings which has less GNSS satellites in sight; The building on the south of Part 5 blocks the south-side satellites; Part 6 is a narrow path surrounded by several buildings which is hardly to see enough satellites for GNSS positioning. Because the RTK receiver was inaccurate in Parts 2 and 6, we used some reference points to mark the true trajectory.

Besides, another 9 MTs were located in the experimental area. MT2-MT4 did circular movements as the yellow lines shown in Fig. 4. And MT5-MT10 were fixed. Some settings and assumptions were made during the experiments except

[5]The D2D measurements are obtained by adding Gaussian noises to the true values, which is calculated by the reference GNSS positions and the simulated trajectories.

$$\Omega_k^{(ij,\gamma)} = \mathrm{diag}\left[\cos\left(y_{\theta,k}^{(ij,\gamma)}\right)\cos\left(y_{\eta,k}^{(ij,\gamma)}\right), \cos\left(y_{\theta,k}^{(ij,\gamma)}\right)\sin\left(y_{\eta,k}^{(ij,\gamma)}\right), \sin\left(y_{\theta,k}^{(ij,\gamma)}\right)\right] \tag{27}$$

$$y_{Z,k}^{(i\mathcal{N}^{(i)},\Im)} = A_{G,k}^{(\mathcal{N}^{(i)},\Im)} \hat{X}_{x,k-1}^{(\mathcal{N}^{(i)})} + \Phi_k^{(\mathcal{N}^{(i)},\Im)} u_{k-1}^{(\mathcal{N}^{(i)})} - D_{D,k}^{(i\mathcal{N}^{(i)},\Im)} \vartheta^{(i\mathcal{N}^{(i)})} \tag{28}$$

$$\begin{aligned}\Psi_k^{(i)} D_{D,k}^{(i\mathcal{N}^{(i)},\Im)} \vartheta^{(i\mathcal{N}^{(i)})} &= \Psi_k^{(i)} \left(\mathring{\Omega}_k^{(i\mathcal{N}^{(i)},\Im)} + \Delta\Omega_k^{(i\mathcal{N}^{(i)},\Im)}\right) C_{D,k}^{(i\mathcal{N}^{(i)},\Im)} \vartheta^{(i\mathcal{N}^{(i)})} \\ &= \Psi_k^{(i)} \mathring{D}_{D,k}^{(i\mathcal{N}^{(i)},\Im)} \vartheta^{(i\mathcal{N}^{(i)})} + \underbrace{\Psi_k^{(i)} \Delta\Omega_k^{(i\mathcal{N}^{(i)},\Im)} C_{D,k}^{(i\mathcal{N}^{(i)},\Im)} \vartheta^{(i\mathcal{N}^{(i)})}}_{=n_{\Psi,k}^{(i)}} = 0\end{aligned} \tag{42}$$

$$\begin{aligned}\Delta\Omega_k^{(ij,\gamma)} \approx\ & \mathrm{diag}\left[-\cos\left(y_{\theta,k}^{(ij,\gamma)}\right)\sin\left(y_{\eta,k}^{(ij,\gamma)}\right), \cos\left(y_{\theta,k}^{(ij,\gamma)}\right)\cos\left(y_{\eta,k}^{(ij,\gamma)}\right), 0\right] n_{y_\eta}^{(ij,\gamma)} \\ & + \mathrm{diag}\left[-\sin\left(y_{\theta,k}^{(ij,\gamma)}\right)\cos\left(y_{\eta,k}^{(ij,\gamma)}\right), -\sin\left(y_{\theta,k}^{(ij,\gamma)}\right)\sin\left(y_{\eta,k}^{(ij,\gamma)}\right), \cos\left(y_{\theta,k}^{(ij,\gamma)}\right)\right] n_{y_\theta}^{(ij,\gamma)}\end{aligned} \tag{49}$$

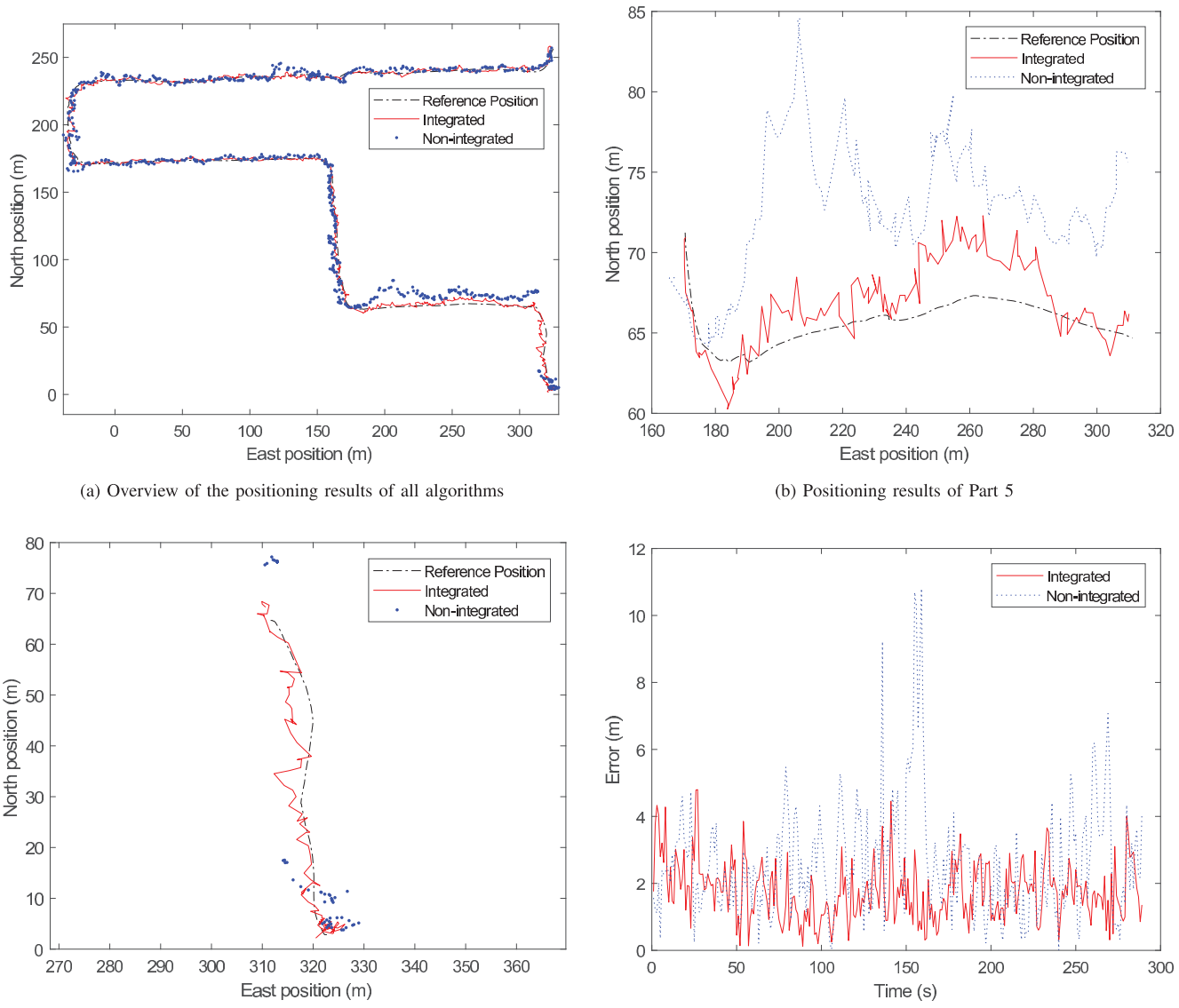

(a) Overview of the positioning results of all algorithms

(b) Positioning results of Part 5

(c) Positioning results of Part 6

(d) Positioning results of Parts 1

Fig. 6. Detailed results of some parts.

stated otherwise:

1) MT2-MT10 output the GNSS positioning results at 1Hz with Gaussian noises of 0 mean and 13m standard deviation;
2) The D2D measurement errors were set to: $\sigma_d = 1$m, $\sigma_\eta = \sigma_\theta = 1^\circ$ and 0 mean Gaussian noise;
3) The time skew and offset of all MTs are unknown. The time skews are randomly set in $[0.99998, 1.00002]$ and the time offsets are randomly set in $[-10, 10]$ ns;
4) There are 2 CF pairs in CO-MWR, namely $\Gamma = 2$;
5) The 5G D2D measure distance is up to 200m;
6) 100 particles are used;
7) Only the line-of-sight (LOS) condition for D2D positioning measure is considered;
8) Only horizontal accuracy is concerned.

The root-mean-square errors (RMSEs) and the RMSE improvement rates (IR) which are calculated by (51) are used to evaluate the performance of the proposed algorithm.

$$\text{Improvement rate} = \left(1 - \frac{\text{RMSE}_{\text{Integrated}}}{\text{RMSE}_{\text{Non-integrated}}}\right) \times 100\% \quad (51)$$

From Fig. 5, it is clear that Parts 1, 3 and 4 have better accuracy either by integrated or non-integrated method because of the good GNSS conditions in these parts; Parts 2 and 5 have high accuracy by integrating D2D signals while low accuracy is achieved by GNSS solely as there are less satellites in sight in these parts which causes the non-integrated method to become worse; There are not fixed solutions by GNSS in Part 6 as there are not enough satellites in-view, while the integrated method does give positioning results. Specifically, the total RMSE (results excluding Part 6) of the integrated method is 56.2% better than the non-integrated method.

Algorithm 3 Integration Algorithm for GNSS/5G D2D Integrated Positioning - Uncertain Time Parameters Scenario

Input: The initial distribution at time slot 0.
Output: The estimate of $\hat{X}_{x,k}^{(i)}$.

1: For each particle $i = 1, 2, \ldots, N_P$, sample the initial state $PX_0^{(i)}(m)$ from the initial distribution $p\left(X_{x,0}^{(i)}\right)$
2: Calculate the weights and normalize them.
3: **for** time slot $k = 1, 2, 3, \ldots$ **do**
4: Sample the particles of time slot k by the importance distribution: $PX_k^{(i)}(m) \sim p\left(X_{x,k}^{(i)} \mid X_{x,k-1}^{(i)}, u_{k-1}^{(\mathcal{N}^{(i)})}\right)$
5: Calculate the orthogonal projection operator: $\Psi_k^{(i)} = I - D_{D,k}^{(i\mathcal{N}^{(i)},\Im)}\left(D_{D,k}^{(i\mathcal{N}^{(i)},\Im)T} D_{D,k}^{(i\mathcal{N}^{(i)},\Im)}\right)^{+} D_{D,k}^{(i\mathcal{N}^{(i)},\Im)T}$
6: Eliminate the time uncertainties: $\Psi_k^{(i)} y_{Z,k}^{(i\mathcal{N}^{(i)},\Im)} = \Psi_k^{(i)}\left(A_{G,k}^{(\mathcal{N}^{(i)},\Im)} \hat{X}_{x,k-1}^{(\mathcal{N}^{(i)})} + \Phi_k^{(\mathcal{N}^{(i)},\Im)} u_{k-1}^{(\mathcal{N}^{(i)})}\right)$
7: Estimate the rough position of MT i: $\tilde{X}_{x,k}^{(i)} = \left(C_k^{(i)T} C_k^{(i)}\right)^{-1} C_k^{(i)T} y_{G,Z,k}^{(i\mathcal{N}^{(i)},\Im)}$
8: Update the distribution of the equivalent measurement noise: $p\left(y_{Gx,k}^{(i)}, \Psi_k^{(i)} y_{Z,k}^{(i\mathcal{N}^{(i)},\Im)} \mid X_{x,k}^{(i)}\right)$ by the distribution of $n_{y_{Gx},k}^{(i)}$, $n_{y_{Gx},k}^{(\mathcal{N}^{(i)},\Im)}$ and $n_{D_D,k}^{(i\mathcal{N}^{(i)},\Im)}$ according to (40) and (50)
9: Calculate the weights: $w_{p,k}^{(i)}(m) \propto p\left(y_{Gx,k}^{(i)}, \Psi_k^{(i)} y_{Z,k}^{(i\mathcal{N}^{(i)},\Im)} \mid X_{x,k}^{(i)}\right)$
10: Normalize the weights: $w_{p,k}^{(i)}(m) = w_{p,k}^{(i)}(m) / \sum_{m=1}^{N_p} w_{p,k}^{(i)}(m)$
11: Resampling and update the particle set $PX_k^{(i)}(m)$, then the weights become: $w_{p,k}^{(i)}(m) = \frac{1}{N_p}$
12: The integrated state is $\hat{X}_{x,k}^{(i)} = \frac{1}{N_p} \sum_{m=1}^{N_p} PX_k^{(i)}(m)$
13: **end for**

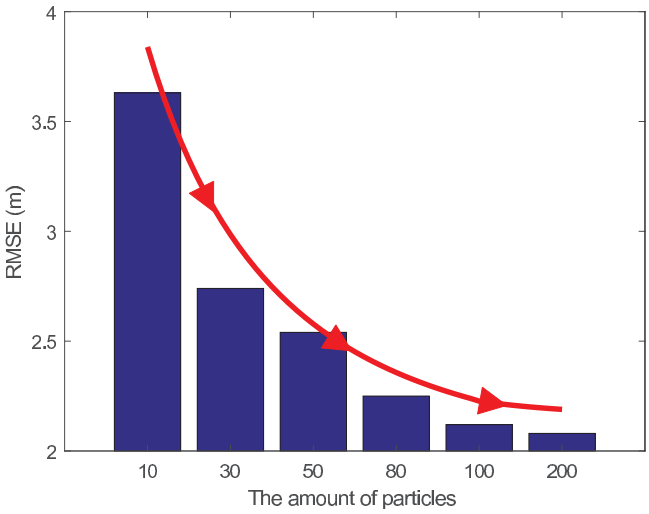

Fig. 7. Impact of the amount of particles on integrated positioning accuracy.

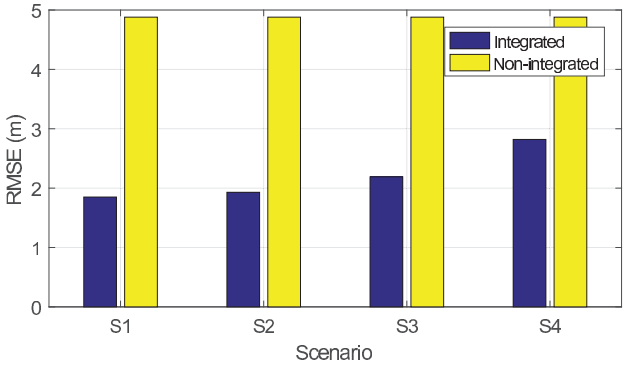

Fig. 8. Impact of D2D measurement accuracy on the positioning accuracy with 100 particles (results without Part 6). S1: $\sigma_d = 50$cm, $\sigma_\eta = \sigma_\theta = 0.5°$; S2: $\sigma_d = 1$m, $\sigma_\eta = \sigma_\theta = 1°$; S3: $\sigma_d = 3$m, $\sigma_\eta = \sigma_\theta = 3°$; S4:$\sigma_d = 5$m, $\sigma_\eta = \sigma_\theta = 5°$.

Detailed analyses are shown in Fig. 6. Fig. 6a shows the overview of the positioning results.

Fig. 6b shows that the non-integrated results have several meters bias from the true trajectory in Part 5. It is because the southern building blocked the southern satellites and the poor horizontal dilution of precision (HDOP) led to north-biased results. While the integrated results are accurate thanks to the correction by D2D measurements. On the other hand, Part 5 has the largest IR than other parts because of the poor GNSS condition as shown in Fig. 5.

Fig. 6c shows the positioning results in GNSS-denied scenario. Notice that the GNSS measurement of MT i ($i = 1$ in this experiment) is not available, so the measurement matrix and the equivalent measurement noise shown in (39) and (40) degenerate to $C_k^{(i)} = \Psi_k^{(i)}\left(\mathbf{1}_{\Gamma(N-1)\times 1} \otimes I_{3\times 3}\right)$ and $n_{y,k}^{(i)} = \Psi_k^{(i)}\left(n_{y_{Gx},k}^{(\mathcal{N}^{(i)},\Im)} + n_{D_D,k}^{(i\mathcal{N}^{(i)},\Im)}\right)$, respectively. Moreover, the velocity measurements in $u_{k-1}^{(i)}$ are also unavailable. As a result, $p\left(X_{x,k}^{(i)} \mid X_{x,k-1}^{(i)}, u_{k-1}^{(i)}\right)$ in (19) degenerates to $p\left(X_{x,k}^{(i)} \mid X_{x,k-1}^{(i)}\right)$. To avoid the impact of the inaccurate process model, the covariance of the process noise should be increased to a certain extent.

From Fig. 6c, we can see that there are no positioning results of GNSS in most time of Part 6, while the integrated algorithms can provide accurate estimates. This means that GNSS/5G integrated positioning[6] has the potential to replace or work with the inertial navigation system (INS) which is widely integrated with GNSS in GNSS-denied environment. Moreover, GNSS/5G D2D integrated positioning is better than GNSS/INS integrated positioning when the initial position is inaccurate or the GNSS is unavailable for a long time.[7]

Fig. 6d shows the positioning errors of Parts 1. Because there are enough satellites and less obstacles, the non-integrated accuracy is only slightly worse than the integrated ones. There are similar results for Part 3 which is not

[6]Because other MTs still need the GNSS results, we do not call it as 5G single positioning in this condition.

[7]Because the INS calculates the position from the former position each time and there will be large accumulated error for a long time [28].

illustrated for saving space. However, the IR of Part 4, which has good GNSS condition as well, is obliviously larger than the ones of Part 1 and 3 as shown in Fig. 5. This is because there are more visible MTs in Part 4 (average 8 visible MTs) than other parts (average 5 and 6 visible MTs in Part 1 and 3, respectively). As a result, much performance improvement is achieved by using more D2D measurements.

Fig. 7 shows the RMSEs with using different amount of particles. It is clear that the positioning accuracy becomes higher with the increasing of the amount of particles. When the amount of particles is larger than 100, the performance improvement is very slightly. Considering the resource consumption, 100 particles are chosen in our experiment.

Fig. 8 illustrates the RMSEs of each algorithms when 5G has different D2D measurement errors if the time skew and offset of all MTs are known. It shows that larger D2D measurement errors lead to larger RMSEs by using the integrated algorithms. However, all integrated ones are much more accurate than the non-integrated ones. Besides, by comparing Fig. 8 and Fig. 5, we can see slightly better positioning performance of the integrated algorithm is achieved with known time parameters as more information is obtained in such condition.

VI. Conclusions

In this paper, we focused on the GNSS/5G integrated positioning methodology with the D2D range and angle measurements. First, according to the features of GNSS/5G integrated positioning network, a novel CO-MWR protocol for D2D positioning measure in 5G communication networks was proposed to improve the measure efficiency without consuming much resources than the conventional TWR protocol. The GNSS 1PPS timing signal was used for a rough synchronization, so that the time stamps need not to be exchanged in the D2D networks and saved significantly resources especially in large-scale networks by utilizing our CO-MWR protocol. Second, the particle filter was employed to estimate the user's state. To tackle the problem of particle degeneracy caused by the high-dimensional state space in the integrated positioning system, we proposed a state dimension reduction method which reduces the state from $6N$ to 3 in the 3-dimensional coordinate. With the proposed integrated algorithm, state estimation method with either certain or uncertain time parameters were explored. In the uncertain time scenario, an orthogonal projection operator was employed to eliminate the time uncertainties. We then derived the alternative measurement noise distribution which was used in PF to improve the filtering performance.

The simulation and experiment results show that the proposed integrated positioning methodology outperforms the non-integrated one especially with more MTs and accurate D2D measurements. Meanwhile, we also designed the integrated positioning algorithm when GNSS is not available which is very common in urban or indoor positioning applications. The integrated results are accurate and robust in these environments as well.

References

[1] D. Pascual, H. Park, A. Camps, A. A. Arroyo, and R. Onrubia, "Simulation and analysis of GNSS-R composite waveforms using GPS and galileo signals," *IEEE J. Sel. Topics Appl. Earth Observ. Remote Sens.*, vol. 7, no. 5, pp. 1461–1468, May 2014.

[2] R. T. Ioannides, T. Pany, and G. Gibbons, "Known vulnerabilities of global navigation satellite systems, status, and potential mitigation techniques," *Proc. IEEE*, vol. 104, no. 6, pp. 1174–1194, Jun. 2016.

[3] Y. Gu, L.-T. Hsu, and S. Kamijo, "GNSS/Onboard inertial sensor integration with the aid of 3-D building map for lane-level vehicle self-localization in urban canyon," *IEEE Trans. Veh. Technol.*, vol. 65, no. 6, pp. 4274–4287, Jun. 2016.

[4] M. Farooq-I-Azam, Q. Ni, and E. A. Ansari, "Intelligent energy efficient localization using variable range beacons in industrial wireless sensor networks," *IEEE Trans. Ind. Informat.*, vol. 12, no. 6, pp. 2206–2216, Dec. 2016.

[5] F. Dovis, B. Muhammad, E. Cianca, and K. Ali, "A run-time method based on observable data for the quality assessment of GNSS positioning solutions," *IEEE J. Sel. Areas Commun.*, vol. 33, no. 11, pp. 2357–2365, Nov. 2015.

[6] C. Zhu and X. Fan, "A novel method to extend coherent integration for weak GPS signal acquisition," *IEEE Commun. Lett.*, vol. 19, no. 8, pp. 1343–1346, Aug. 2015.

[7] D. Zhongliang, Y. Yanpei, Y. Xie, W. Neng, and Y. Lei, "Situation and development tendency of indoor positioning," *Commun., China*, vol. 10, no. 3, pp. 42–55, Mar. 2013.

[8] C.-H. Ko and S.-H. Wu, "A proactive indoor positioning system in randomly deployed dense WiFi networks," in *Proc. IEEE Global Commun. Conf. (GLOBECOM)*, Dec. 2016, pp. 1–6.

[9] F. Xie, J. Liu, R. Li, and Y. Hang, "Adaptive robust ultra-tightly coupled global navigation satellite system/inertial navigation system based on global positioning system/Beidou vector tracking loops," *IET Radar, Sonar Navigat.*, vol. 8, no. 7, pp. 815–827, Aug. 2014.

[10] X. Cui, T. A. Gulliver, J. Li, and H. Zhang, "Vehicle positioning using 5G millimeter-wave systems," *IEEE Access*, vol. 4, pp. 6964–6973, 2016.

[11] X. Cui, T. A. Gulliver, H. Song, and J. Li, "Real-time positioning based on millimeter wave device to device communications," *IEEE Access*, vol. 4, pp. 5520–5530, 2016.

[12] J. A. del Peral-Rosado, J. A. López-Salcedo, S. Kim, and G. Seco-Granados, "Feasibility study of 5G-based localization for assisted driving," in *Proc. IEEE Int. Conf. Localization ICL-GNSS*, 2016, pp. 1–6.

[13] A. Dammann, T. Jost, R. Raulefs, M. Walter, and S. Zhang, "Optimizing waveforms for positioning in 5G," in *Proc. IEEE 17th Int. Workshop Signal Process. Adv. Wireless Commun. (SPAWC)*, Jul. 2016, pp. 1–5.

[14] J. Werner, M. Costa, A. Hakkarainen, K. Leppanen, and M. Valkama, "Joint user node positioning and clock offset estimation in 5G ultra-dense networks," in *Proc. IEEE Global Commun. Conf. (GLOBECOM)*, Dec. 2015, pp. 1–7.

[15] A. Dammann, R. Raulefs, and S. Zhang, "On prospects of positioning in 5G," in *Proc. IEEE Int. Conf. Commun. Workshop (ICCW)*, Jun. 2015, pp. 1207–1213.

[16] S. Thrun, W. Burgard, and D. Fox, *Probabilistic Robotics*. Cambridge, MA, USA: MIT Press, 2005.

[17] R. Shafin, L. Liu, Y. Li, A. Wang, and J. Zhang, "Angle and delay estimation for 3-D massive MIMO/FD-MIMO systems based on parametric channel modeling," *IEEE Trans. Wireless Commun.*, vol. 16, no. 8, pp. 5370–5383, Aug. 2017.

[18] Y. Zhou, Z. Fei, S. Yang, J. Kuang, S. Chen, and L. Hanzo, "Joint angle estimation and signal reconstruction for coherently distributed sources in massive MIMO systems based on 2D unitary ESPRIT," *IEEE Access*, 2017.

[19] *IEEE Computer Society Standard*, document IEEE Standard 802.15.4a-2007.

[20] B. Siciliano and O. Khatib, *Springer Handbook of Robotics*. Springer, 2016.

[21] J. Míguez, D. Crisan, and I. P. Mariño, "Particle filtering for Bayesian parameter estimation in a high dimensional state space model," in *Proc. 23rd IEEE Eur. Signal Process. Conf. (EUSIPCO)*, Aug. 2015, pp. 1241–1245.

[22] B. Ait-El-Fquih and I. Hoteit, "A variational Bayesian multiple particle filtering scheme for large-dimensional systems," *IEEE Trans. Signal Process.*, vol. 64, no. 20, pp. 5409–5422, Oct. 2016.

[23] S. Ganeriwal, R. Kumar, and M. B. Srivastava, "Timing-sync protocol for sensor networks," in *Proc. Int. Conf. Embedded Netw. Sensor Syst.*, 2003, pp. 138–149.
[24] T. Zheng, M. Gidlund, and J. Akerberg, "WirArb: A new MAC protocol for time critical industrial wireless sensor network applications," *IEEE Sensors J.*, vol. 16, no. 7, pp. 2127–2139, Apr. 2016.
[25] S. Zhu and Z. Ding, "Joint synchronization and localization using TOAs: A linearization based WLS solution," *IEEE J. Sel. Areas Commun.*, vol. 28, no. 7, pp. 1017–1025, Sep. 2010.
[26] W. Yuan, N. Wu, B. Etzlinger, H. Wang, and J. Kuang, "Cooperative joint localization and clock synchronization based on Gaussian message passing in asynchronous wireless networks," *IEEE Trans. Veh. Technol.*, vol. 65, no. 9, pp. 7258–7273, Sep. 2016.
[27] S. He and X. Dong, "High-accuracy localization platform using asynchronous time difference of arrival technology," *IEEE Trans. Instrum. Meas.*, vol. 66, no. 7, pp. 1728–1742, Jul. 2017.
[28] D. H. Won *et al.*, "Selective integration of GNSS, vision sensor, and INS using weighted DOP under GNSS-challenged environments," *IEEE Trans. Instrum. Meas.*, vol. 63, no. 9, pp. 2288–2298, Sep. 2014.

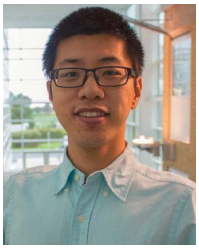

Lu Yin (M'17) received the B.Sc. and Ph.D. degrees in electrical engineering from the Beijing University of Posts and Telecommunications (BUPT), Beijing, China, in 2014. He was an Academic Visitor with the InfoLab21, Lancaster University, from 2016 to 2017. He is currently an Assistant Professor with the School of Electronic Engineering, BUPT. His current research interests are in the areas of global navigation satellite system, indoor positioning, integrated/cooperative positioning, intelligent localization, and communication system.

Qiang Ni (M'04–SM'08) received the B.Sc., M.Sc., and Ph.D. degrees in engineering from the Huazhong University of Science and Technology, China. He is currently a Professor and the Head of the InfoLab21, Communication Systems Group, School of Computing and Communications, Lancaster University, Lancaster, U.K. His main research interests lie in the area of future generation communications and networking, including green communications and networking, cognitive radio network systems, heterogeneous networks, small cell and ultra-dense networks, 5G, SDN, cloud networks, energy harvesting, wireless information and power transfer, Internet of Things, and vehicular networks. He has authored or co-authored over 180 papers in these areas. He was the IEEE 802.11 Wireless Standard Working Group Voting Member and a contributor to the IEEE Wireless Standards.

Zhongliang Deng received the M.Sc. degree in manufacturing engineering from Beihang University and the Ph.D. degree in mechanical manufacture from Tsinghua University, China. During 2002–2003, he was the Senior Visiting Scholar with Southern California University, Los Angeles, CA, USA. Since 2006, he has been holding the position of director of research with the Laboratory of Intelligent Communication, Navigation and Micro/Nano-Systems. He is currently a Professor and a Doctoral Supervisor with the School of Electronic Engineering, Beijing University of Posts and Telecommunications. His research interests include indoor and outdoor seamless positioning, global navigation satellite system, satellite communications, MEMS, and multimedia.